Study on Optimization of Silty Sand Soil Properties by Graphene Oxide-Silica Fume Modified Cement-based Materials

Yahui Ma [1,2], Baoguo Pei [1],Yuwen Ju [2*]

[1] Taiyuan Rail Transit Group Co., LTD., Taiyuan 030032, China
[2] Civil Engineering College, Taiyuan University of Technology, Taiyuan 030024, China

E-mail:418171839@qq.com

Abstract. In the context of rapid urbanization and industrialization, subterranean engineering frequently encounters geotechnical challenges, particularly when dealing with weak soil layers, such as loose silty sand. These layers are problematic due to their poor permeability and low mechanical strength. Although cement-based solidification methods are prevalent for improving soil properties, they may prove inadequate under certain extreme conditions. This study explores the solidification efficacy of graphene oxide (GO) alone, and in conjunction with silica fume (SF), on silty sand by integrating varying proportions of GO and SF into cement-based composite materials, with a focus on assessing their influence on the impermeability and mechanical properties of the solidified soil. The findings revealed that the incorporation of GO alone markedly decreased the permeability coefficient and enhanced the early bending and compressive strength of the solidified soil. Optimal impermeability and mechanical performance were attained at a GO concentration of 0.06%, attributed to GO's high specific surface area and superior adsorption capacity, which effectively filled internal soil voids and ameliorated the microstructure. When GO and SF were added together, the solidified soil's performance improved, especially at an SF content of 10%. Notably, even with reduced GO content, a significant decrease in permeability coefficient was observed, indicating a synergistic effect between the materials. The concurrent addition of GO and SF also had a positive impact on bending and compressive strength, notably enhancing the early and intermediate mechanical performance of the solidified matrix. After a curing period of 28 days, the growth trends of bending and compressive strength decelerated. Microscopic examination indicated that GO and SF addition optimized the pore structure of the solidified soil, diminishing macropores and augmenting micropores, thereby reducing the permeability coefficient and bolstering impermeability. X-ray diffraction (XRD) analysis demonstrated that although the addition of GO and SF did not alter the primary hydration products in the solidified soil, it facilitated the cement hydration reaction, leading to increased formation of hydrated calcium silicate gels and other hydration products, thereby enhancing the compactness and mechanical strength of the solid matrix.

Keywords: graphene oxide; silica fume; cement-based materials; silty sand body; impermeability; mechanical properties; microstructure

B. Yuan et al. (eds.), *Proceedings of the 2024 8th International Conference on Civil Architecture and Structural Engineering (ICCASE 2024)*, Atlantis Highlights in Engineering 33,
https://doi.org/10.2991/978-94-6463-449-5_49

1 INTRODUCTION

With the rapid development of national economic construction, the speed, type and scale of various underground engineering construction in China are also developing vigorously with an unprecedented attitude[1-3]. The scope of infrastructure construction is continuously expanding, leading to the inevitable encounter with various types of soft soil layers in practical engineering. Among these, the silty soil layer is particularly problematic, as its poor impermeability and low shear strength make it prone to water seepage in deep excavation support, underground spaces, and other structural projects [4,5]. In soft soil solidification technology, cement is the material of choice [6], particularly for engineering applications focused on water stoppage and seepage control. In practical engineering, the effectiveness of soft soil stratum solidification using grouting materials is assessed not only by the strength of the consolidated body but also by its impermeability and durability [7]. Among cement grouting materials, due to their low cost, high stability, and widespread availability, and the ability to be enhanced with additives like bentonite, lime powder, silica fume, fly ash, and blast furnace slag, not only is the performance of the grout improved, but the cost of grouting is also reduced, alleviating environmental pressure from industrial waste. The strategic use of industrial waste residues in cement-based materials fosters resource conservation and environmental protection. Simultaneously, it promotes the innovation and advancement of grouting technology, contributing to the achievement of carbon peaking and carbon neutrality objectives [8].

SF is a by-product formed during the manufacturing of metallic silicon or ferrosilicon alloys in electric arc furnaces [9].Due to its superior physical and chemical properties, SF has been extensively utilized as an admixture in cement mortar and concrete [10-13]. Nasr et al. [14] analyzed the impact of high silica fume content on the mechanical properties and durability of cement mortar. They found that incorporating a high proportion of silica fume significantly enhanced the mechanical performance and durability of the cement mortar. The study also highlighted that silica fume improves the overall performance of the material by increasing the micro-density of the cement mortar and enhancing the hydration reaction. Jiang et al. [15] studied the effect of ultrafine wollastonite powder on the properties of cement-based materials. They discovered that incorporating ultrafine wollastonite powder significantly improved the compressive and flexural strength of cement materials, while also enhancing their durability. The study explained that ultrafine wollastonite powder enhances the overall performance of the material by promoting the hydration reaction of cement and optimizing the microstructure of cement-based materials. He et al. [16] explored the impact of silica fume as an admixture on the impermeability and mechanical properties of cement-based cutoff walls. Their research found that adding silica fume significantly improved the impermeability of the cutoff walls. This improvement is attributed to the fine particles in silica fume filling the micro-pores in the cement-based materials, reducing porosity, and thereby decreasing permeability.

In recent years, the incorporation of nano-materials into cement-based materials has sparked significant interest among researchers[17,18].GO is notably characterized by its large specific surface area, with its lamellar edges and surfaces being rich in oxygen-

containing functional groups [19].Scholars have incorporated GO as an admixture in cement-based materials, conducting extensive research on enhancing the mechanical properties and durability of cement-based composites[20-23]. Mokhtar et al. [24] investigated the reinforcing effect of graphene oxide nano-sheets on cement-based materials and their mechanism of action. The addition of graphene oxide nano-sheets significantly improved the mechanical properties of cement-based materials, including compressive strength, tensile strength, and flexural strength. It also enhanced the durability and crack resistance of the materials, reducing structural damage. Mohammed et al. [25], through further research, found that the addition of graphene oxide can reduce the porosity of cement-based materials, thereby decreasing the permeability of water and other harmful substances. This improvement is primarily attributed to the microstructural network formed by graphene oxide within the cement matrix, which enhances the microstructure of the material and improves its compactness. However, the majority of these studies have concentrated on the effects of single GO blending, with a lack of systematic research on the properties of cement-based materials under various blending conditions. Future research should aim to more comprehensively assess the influence of GO on the properties of cement-based materials, with a particular focus on its role in multi-component composite systems.

Since the 1970s, significant advancements have been achieved in the research on the application of cement-solidified soil. Currently, the studies concerning the mechanical properties, deformation characteristics, and microscopic mechanisms of cement-solidified soil have reached a mature stage. This material is extensively utilized in foundation anti-seepage projects, demonstrating its vast potential for application. In recent years, researchers both domestically and internationally have extensively investigated the mechanical properties and impermeability of cement-solidified soil [26-28], aiming to enhance its value for engineering applications.

Therefore, this study focuses on silty sand as the subject, solidifying it by incorporating cement and various additives. Laboratory tests were conducted to examine the impact of GO and a combination of GO/SF on the permeability coefficient and mechanical strength of the solidified bodies created with cement-based materials. Techniques such as nuclear magnetic resonance (NMR), scanning electron microscopy, and X-ray diffraction (XRD) were employed to investigate the solidification mechanisms of water-cement-based materials modified with GO and SF.

2 TEST

2.1 Test Material

The cement used in the study is P.O 42.5 ordinary Portland cement, manufactured by Taiyuan Shitou Cement Co., Ltd., with its main parameters detailed in Table 1. GO, acquired in a solution state with a concentration of 10mg/ml, is industrial-grade single-layer GO from Suzhou Carbon Graphene Technology Co., Ltd., with some of its physical properties listed in Table 2. Silica fume, produced by Gongyi City Baichuan Environmental Protection Engineering Co., Ltd., also has its primary parameters presented

in Table 1. The soil material for the study was sourced from the Liuxiang subway station excavation site in Taiyuan, subsequently dried, pulverized, and sieved through a 2mm mesh to prepare the test soil. The basic physical properties of the utilized silty sand are provided in Table 3, with the water content of the test soil determined to be 20.30%. The water glass solution, produced by Wuxi Yatai United Chemical Co., Ltd., has a density of 1.38 g/ml, a modulus of 2.4, and a concentration of 50° Bé, which was diluted to 35° Bé prior to testing. Distilled water was used for the tests.

Table 1. Chemical components of cement and silica fume

Material	Mass fraction/(%)							
	SiO_2	Al_2O_3	CaO	Fe_2O_3	MgO	SO_3	Na_2O	Loss
Cement	24.99	8.26	53.84	4.03	3.71	2.51	0.35	2.31
Silica fume	96.16	0.30	0.03	0.07	0.10	-	0.08	-

Table 2. Physical parameters of graphene oxide

Morpho-logical	Fine-ness	Lay-ers	Layer Diameter	Thick-nesses	Carbon content	Oxygen content	Sulphur content
liquid	>95%	1-2	10-50μm	~1nm	<50%	>42%	<4%

Table 3. Basic physical indicators of experimental soil

Water content (%)	Natural density (g/cm^3)	Pore ratio	Liquid limit w_L(%)	Plastic limit w_P(%)	Plasticity index I_p	Permeability coefficient (10^{-6}cm/s)
20.30	1.88	0.77	22.52	15.21	7.31	23.95

2.2 Test Scheme

The experiment focused on assessing the impermeability and mechanical properties of silty sand particle solidified bodies using cement-based grouting materials modified with a GO-SF blend, which represent critical engineering performance indicators of cement-soil composites. Consequently, the primary tests conducted included the permeability coefficient test, flexural strength test, and compressive strength test. To elucidate the impact of GO alone and in combination with SF on the impermeability and mechanical properties, a detailed and rational mix ratio scheme was established. Based on prior experimental data, the water-to-cement ratio was set at 0.4, with the water glass solution constituting 50% of the cement's volume fraction, and cement making up 50% of the silty sand particles' mass fraction. Drawing from extensive prior research, the GO content was determined to be 0.03%, 0.06%, and 0.09% of the total mass of the cement slurry, while the SF content was set at 0%, 6%, 8%, and 10% of the cement's mass.

2.3 Preparation of Sample

The impermeability test adopts φ 50mm × H 50mm three-lobe die, and the strength test adopts 40mm × 40mm × 160mm triple prism die.

According to the test plan, the pre-weighed cement, SF, and silty sand particles are placed into a mortar mixer and mixed for 60 seconds to ensure thorough blending. The corresponding GO solution is then dispersed into 80% of the test water and subjected to ultrasonic dispersion for 10 minutes. Subsequently, this GO solution, along with the remaining water and the specified sodium silicate solution, are added to the mortar mixer and stirred for 180 seconds to achieve uniform consistency. The mixture is then poured into the prepared plastic mold in three layers and vibrated on a vibration table for 1 minute to ensure that the slurry uniformly and densely fills the mold. The surface of the mold is leveled with a scraper, and the test block is placed in a standard curing box to cure. The permeability tests are conducted at 12 and 24 hours, while the strength tests are carried out at 3, 7, and 28 days. Each test is conducted with three parallel samples to ensure consistency and reliability of the results.

2.4 Test Method

Permeability Test.

The permeability coefficient is a key metric for assessing the water-conducting capacity of soil, indicating the ease with which water can pass through the soil matrix. In cement-stabilized soil, the permeability coefficient plays a pivotal role, impacting not only the stability and durability of engineering structures but also bearing significance for environmental protection and sustainable development. By controlling and optimizing the permeability characteristics of cement-stabilized soil, enhanced application outcomes can be achieved in civil engineering practices. PN3230M environmental geotechnical flexible wall penetrometer is used for permeability test.

After saturation using a vacuum saturation device, the osmotic test is conducted at four different osmotic pressures: 100 kPa, 150 kPa, 200 kPa, and 250 kPa, with the confining pressure set to exceed the osmotic pressure by 50 kPa. Once the permeation rate stabilizes, the permeation rates under the four pressure differentials are measured and recorded in accordance with the standard ASTM-D5084-10. The permeability coefficient k ($cm \cdot s^{-1}$) is then calculated using equation (1):

$$k = \frac{\Delta Q \mathrm{L} \rho \mathrm{g}}{\mathrm{A} \Delta P \Delta t} \tag{1}$$

Where: ΔQ is the seepage flow within the time Δt used for seepage, cm^3; L is the height of the test block, cm; ρ is the density of water at 4°C, g/cm^3; g is gravitational acceleration, N/kg; A is the cross-sectional area of the test block, cm^2; ΔP is the pressure corresponding to head difference, kPa.

Because the viscous force of water will be affected by the ambient temperature, it is necessary to convert the calculated permeability coefficient k into 20°C permeability coefficient k_{20}, which is converted according to equations (2) and (3).

$$k_{20} = R_{\mathrm{T}} \times k \tag{2}$$

$$R_{\mathrm{T}} = 2.2902(0.9842^{T})/T^{0.1702} \tag{3}$$

Where: k_{20} is the modified permeability coefficient of 20°C, cm/s; R_{T} is the correction coefficient of water temperature 20°C; T is the water temperature during infiltration, °C.

Strength Test.

In cement-stabilized soil, mechanical strength plays a crucial role, significantly impacting the material's load-bearing capacity and structural stability, while also being vital for enhancing the durability of the project and environmental sustainability. The chemical reaction between cement and soil leads to the formation of a high-strength structure in the stabilized soil, which can effectively withstand substantial loads and resist environmental degradation, thereby maintaining long-term structural integrity. Therefore, precise control of the mechanical strength in cement-stabilized soil is essential for ensuring the quality of the engineering project and safeguarding environmental protection. DYE-300S computer automatic constant stress flexural and compressive testing machine produced by Wuxi Dejiayi Test Instrument Co., Ltd. was used for strength test.

Strength test shall be carried out according to the method specified in standard GB/T17671-2021. Firstly, the surface of the test block is wiped clean, and the flexural strength is tested at a loading speed of 50 N/s until the test block is destroyed; Immediately, the compressive strength of the broken test block was tested at a loading speed of 2.4 kN/s until the test block was destroyed, and the experimental data were screened according to the specification requirements. Samples were taken from the center of the compressive crushing specimen to prepare for the subsequent scanning electron microscope test and X-ray diffraction test.

Microscopic Experiment.

To investigate the pore size and distribution within the solidified body as well as its chemical composition, microscopic experiments were conducted using X-ray diffraction and nuclear magnetic resonance tests. The XRD analysis was performed using a Malvern PANalytical Aeries X-ray diffractometer, while the NMR tests were carried out using a porous media flow-solid coupling analysis and imaging system.

3 RESULTS AND ANALYSIS

A total of 14 groups of proportioning tests were set up, and the test results were shown in Table 4, in which C1 and C2 were control tests.

Table 4. Test results

Group	GO(%)	SF(%)	Permeability coefficient (10^{-8}cm/s)		Flexural strength(MPa)			Compressive strength(MPa)		
			12h	24h	3d	7d	28d	3d	7d	28d
C 1	0	0	7.79	5.77	2.04	3.11	4.22	5.44	7.98	11.65
C 2	0	10	3.83	2.86	2.85	4.19	5.40	8.25	10.65	15.77
G 1	0.03	0	6.64	4.85	2.13	3.22	4.43	6.16	8.62	12.81
G 2	0.06	0	4.82	3.44	2.40	3.71	5.08	7.09	9.26	14.82
G 3	0.09	0	3.80	2.53	2.58	3.55	4.84	7.78	10.03	13.55
G 4	0.03	6	4.47	3.06	2.55	3.74	4.92	7.63	9.21	14.60
G 5	0.06	6	3.12	2.17	2.91	4.32	5.38	8.50	10.84	16.47

G 6	0.09	6	2.07	1.50	3.10	4.12	5.15	9.33	11.64	15.76
G 7	0.03	8	3.31	2.33	2.91	4.08	5.41	8.02	10.14	15.83
G 8	0.06	8	2.32	1.61	3.32	4.45	5.92	9.04	11.92	18.14
G 9	0.09	8	1.41	0.94	3.50	4.71	5.67	9.64	12.80	17.11
G 10	0.03	10	2.88	1.82	3.14	4.32	5.63	8.66	10.95	16.47
G 11	0.06	10	1.60	1.14	3.55	4.73	6.17	9.58	12.92	19.23
G 12	0.09	10	0.91	0.61	3.76	4.94	5.92	10.34	13.95	18.25

3.1 Effect of Single Doping GO on Properties of Consolidated Body

Influence and Analysis of GO single Doping on Permeability Coefficient of Seepage Consolidation Body.

Fig. 1 illustrates the permeability coefficient of consolidated samples at different curing ages with varying GO concentrations. The figure indicates that the permeability coefficient of the consolidated body decreases with an increase in GO content for curing ages of 12 hours and 24 hours. Specifically, at a GO content of 0.03%, the permeability coefficients of the solidified body at 12 hours and 24 hours curing ages decrease by 14.76% and 15.94%, respectively, compared to the C1 control group. With a 0.06% GO content, the reductions in permeability coefficient are 38.13% and 40.38%, respectively. At a 0.09% GO content, the permeability coefficient decreases by 51.22% and 56.15%, respectively. However, when the GO content exceeds 0.06%, the rate of decrease in permeability coefficient begins to slow down, suggesting that the impact of GO on reducing the permeability of the consolidated body tends to stabilize beyond this concentration.

The analysis indicates that GO efficiently fills the pores within the consolidated body, thereby enhancing its compactness and improving its microstructure, which in turn effectively inhibits the creation or expansion of seepage channels. Due to its high specific surface area and adsorption capacity, GO can adsorb water molecules, impeding their movement and diffusion within the consolidated body, and consequently reducing its permeability coefficient. Furthermore, an appropriate quantity of GO can be uniformly distributed in the grouting materials. GO not only facilitates the cement hydration reaction through its abundant functional groups but also forms strong bonds with hydration product gels in various regions, courtesy of its extensive lamellar structure. This interaction significantly enhances the cohesive integration of hydration products across different regions, thereby improving the overall structural integrity of the solidified body.

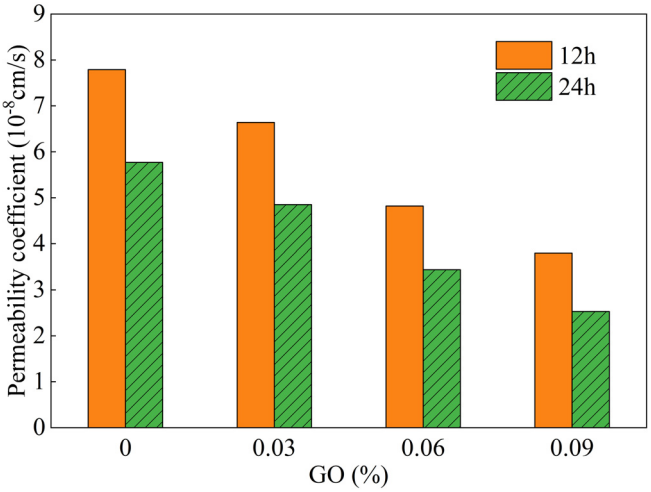

Fig. 1. Variation of solid permeability coefficient with GO single doping admixture

Influence and Analysis of GO Single Addition on the Permeability and Mechanical Strength of Solidified Bodies.

(1) Influence of Single Doping GO on Flexural Strength.

Fig. 2 presents the flexural strength of consolidated samples at varying curing ages, corresponding to different GO concentrations. The figure demonstrates that the flexural strength of the consolidated body samples increases with the rising content of GO at a 3 days curing age. Specifically, for the G1, G2, and G3 groups, the increase in flexural strength compared to the C1 control group is 4.41%, 17.65%, and 26.47%, respectively. However, when the GO content exceeds 0.06%, the rate of increase in flexural strength of the consolidated body samples begins to plateau. For the 7 days and 28 days curing periods, the flexural strength of the consolidated samples initially increases and then decreases with the increasing content of GO, peaking at a GO content of 0.06%. At this concentration, the flexural strength of the 7 days and 28 days consolidated specimens reaches maximum values of 3.71 MPa and 5.08 MPa, respectively, marking increases of 19.29% and 20.38% compared to the C1 control group.

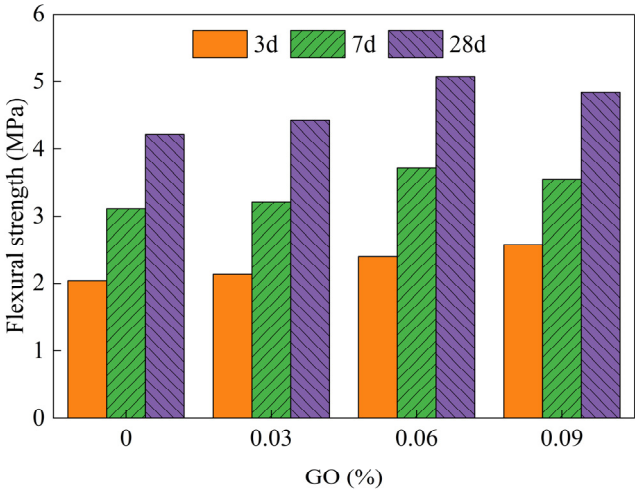

Fig. 2. Variation of flexural strength of solid with single doping admixture of GO

(2) Influence of Single Doping GO on Compressive Strength.

Fig. 3 illustrates the compressive strength of the consolidated body at various curing ages with changes in the GO content. The data, as shown in Fig. 3, reveal that with an increase in GO content, the compressive strength of the consolidated body at 3 days and 7 days curing ages also rises. Specifically, for the G1, G2, and G3 groups, the increase in compressive strength at 3 days and 7 days is 13.24%, 30.33%, and 43.01%, and 8.02%, 16.04%, and 25.7% respectively, compared with the C1 control group. However, as the curing age progresses, the rate of increase in compressive strength for the consolidated body samples begins to decelerate. Regarding the 28 days curing age, the compressive strength of the consolidated body initially increases with the rising content of GO and then decreases, peaking at a GO content of 0.06%. At this concentration, the compressive strength of the consolidated body attains its maximum value, which is 27.21% higher than the C1 control group. When the GO content reaches 0.09%, the compressive strength of the consolidated body is still 16.31% higher than that of the C1 control group, indicating a nuanced response of the material's strength to varying GO concentrations over time.

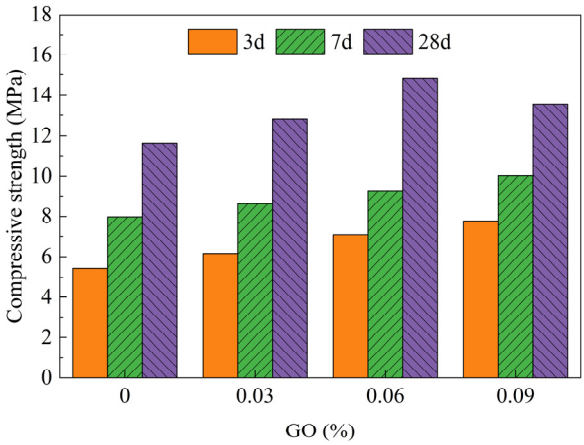

Fig. 3. Variation of compressive strength of solidified body with single doping admixture of GO

(3) Analysis of the Influence of GO Alone on the Mechanical Strength.

The incorporation of GO notably enhances the flexural and compressive strengths of the consolidated body in its early stages. This improvement is attributed to the abundant oxygen-containing functional groups on the surface of GO, which offer numerous reaction sites for the hydration process, thereby accelerating it and rapidly boosting the early strength of the consolidated body. Moreover, the high elastic modulus and tensile strength of GO further strengthen the early mechanical properties of the consolidated body. The two-dimensional layered structure of GO serves as a scaffold during the hydration process, aiding in the formation of more regular and compact hydrated products. This structural influence enhances the material's microstructure density, thereby augmenting the mechanical properties of the consolidated body. Additionally, as a nanomaterial, GO has a small size that enables it to effectively fill micro-cracks and micropores within the consolidated body. This filling action reduces the porosity of the structure, consequently improving the mechanical properties of the consolidated body.

When the GO content increases from 0.06% to 0.09%, a decline in the flexural and compressive strengths of the consolidated sample at 28 days is observed, which could be attributed to the propensity of excessive GO to absorb substantial amounts of water. This absorption can diminish the fluidity of the cement slurry, hinder the thorough vibration of the consolidated sample, and result in an increase in the internal porosity of the sample. Additionally, the large specific surface area of GO facilitates easy agglomeration; as its content rises, its uniform dispersion diminishes, leading to inferior interfacial properties between the GO and the cement paste. Furthermore, the Van der Waals forces between the GO nano-sheets tend to cause aggregation at higher contents, which introduces structural defects in the consolidated body. This poor dispersion also diminishes the ability of GO to facilitate the hydration reaction. The cumulative effect of these factors suggests that an excessive addition of GO can undermine its capacity to enhance the mechanical properties of the consolidated material.

3.2 Effect of GO/SF Composite Addition on the Properties of Solidified Bodies

Influence and Analysis of GO/SF Blending on Permeability Coefficient of Consolidated Body.

Fig. 4 depicts the effect of the combined content of GO and SF on the permeability coefficient of consolidated samples at various curing ages. The data indicate a general downward trend in the permeability coefficient of the consolidated body as the content of GO and SF increases. Notably, when the SF content reaches 10%, a substantial decrease in the permeability coefficient is observed even at a low GO content (0.03%), compared to using GO alone. The most pronounced reduction in the permeability coefficient of the consolidated body occurs at 12 hours and 24 hours when the GO content is increased to 0.09%. This suggests that within a certain range, augmenting the levels of GO and SF can effectively diminish the permeability coefficient.

The combined addition of GO and SF significantly reduces the permeability coefficient of the consolidated body in the initial stage. GO, with its fine particles, effectively fills micro-pores and micro-cracks among soil particles, as well as between soil particles and hydration products. SF, on the other hand, fills larger pores and cracks that GO cannot, thereby enhancing the density of the consolidated body and lowering its permeability coefficient. Moreover, GO aids in the hydration reaction of cement, leading to the formation of numerous flaky calcium hydroxide crystals and contributing to a more compact structure by influencing the arrangement of hydration products. Concurrently, the presence of SF hastens the consumption of calcium hydroxide crystals and leads to the formation of hydrated calcium silicate gel with improved crystallinity, which in turn decreases the porosity of the consolidated body. As a result, there is a macroscopic reduction in the permeability coefficient of the consolidated body.

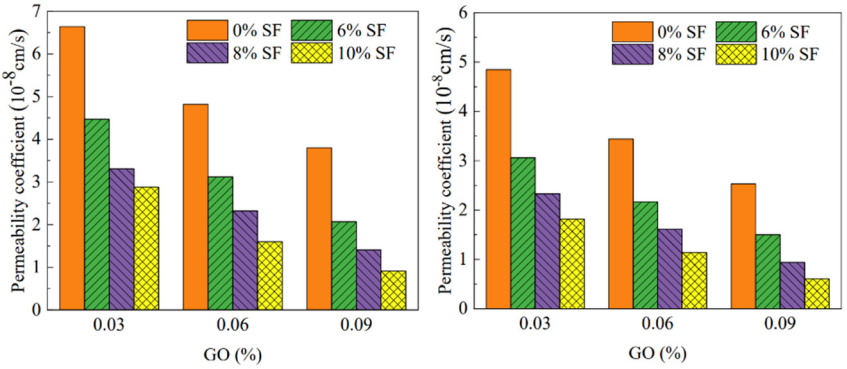

Fig. 4. Variation of solid permeability coefficient with GO/SF compounding dosage

Effect of GO/SF Blending on Mechanical Strength of Consolidated Mass.

(1) The Influence of GO/SF Blending on the Flexural Strength of Consolidated Body.

Fig. 5 shows the influence of GO/SF content on the flexural strength of consolidated samples at different curing ages.

Fig. 5 (a) reveals that, with a constant SF content, the flexural strength of consolidated samples at the 3 days curing age increases as the content of GO rises. Notably, when the SF content is 10% and the GO content is 0.09%, the flexural strength of the consolidated samples at a 3 days curing age reaches its peak, exhibiting an increase of 84.31% compared to the C1 control group, 31.93% compared to the C2 control group, and 45.74% compared to the G3 group.

From Fig. 5 (b), it is observed that as the content of GO increases, the flexural strength of the 7 days consolidated body initially rises and then declines when the SF content is 0% and 6%. However, with SF contents of 8% and 10%, the flexural strength of the consolidated body consistently increases. This trend suggests that an appropriate addition of SF can effectively compensate for the shortcomings of GO in enhancing the flexural strength of the 7 days consolidated body. When the SF content is 10% and the GO content is 0.09%, the flexural strength of the consolidated body peaks, showing an increase of 58.84% compared to the C1 control group, 17.90% compared to the C2 control group, and 39.15% compared to the G3 group. However, this increase is less than the rate of increase in flexural strength observed at 3 days of age.

Fig. 5 (c) shows that with a constant content of SF, the flexural strength of the consolidated body at 28 days of age initially increases and then decreases with the rising content of GO. The peak flexural strength is attained when the GO content is 0.06%. Specifically, at a GO content of 0.06%, and SF contents of 6%, 8%, and 10%, the flexural strength of the consolidated body increases by 5.91%, 16.54%, and 21.46% respectively, compared to the flexural strength of the consolidated body without SF. Furthermore, with GO content at 0.06% and SF at 10%, the flexural strength of the consolidated body at 28 days of age reaches its maximum, showing an increase of 45.21% compared with the C1 control group, 14.26% compared with the C2 control group, and 21.46% compared with the G2 group.

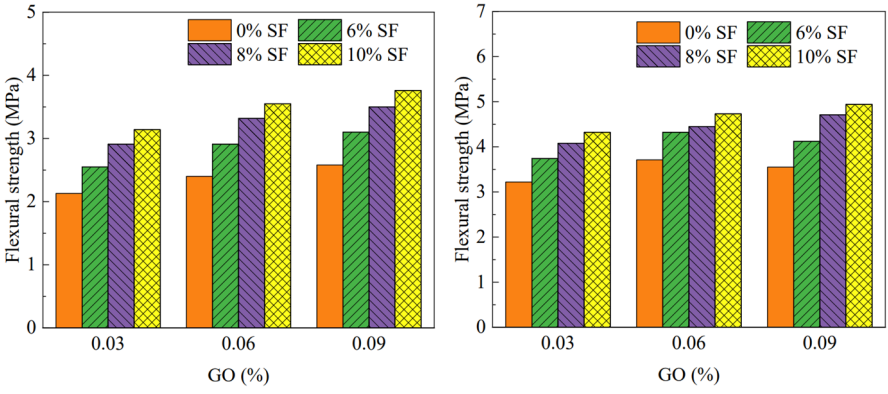

(a) 3d (b) 7d

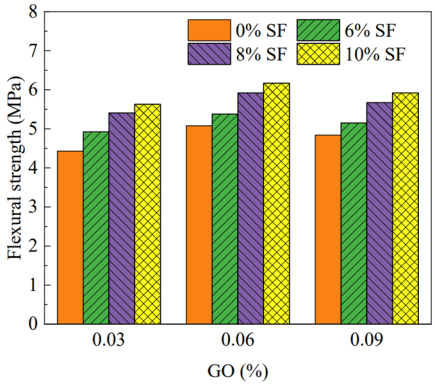

(c) 28d

Fig. 5. Variation of flexural strength of solid with GO/SF compounding dosage

(2) Effect of GO/SF Blending on Compressive Strength of Consolidated Body.

Fig. 6 shows the influence of GO/SF content on the compressive strength of consolidated samples at different curing ages.

Fig. 6 (a) illustrates that with a constant SF content, the compressive strength of consolidated samples at a 3 d curing age increases as the GO content rises. Notably, when the SF content is 10% and the GO content is 0.09%, the compressive strength of the consolidated samples at 3 days of curing reaches its maximum. This strength is 90.07% higher than that of the C1 group, 25.33% higher than that of the C2 control group, and 32.90% higher than that of the G3 group.

Fig. 6 (b) reveals that with a constant content of SF, the compressive strength of the consolidated body at 7 d of age increases with the rising GO content, differing from the flexural strength trend observed at the same age. Specifically, when the SF content is 10% and the GO content is 0.09%, the compressive strength of the consolidated body attains its maximum value. This represents an increase of 74.81% compared with the C1 control group, 30.99% compared with the C2 control group, and 39.08% compared with the G3 group.

Fig. 6 (c) shows that with a constant SF content, the compressive strength of the consolidated body at 28 d of age initially increases and then decreases as the content of GO increases. The optimum compressive strength is achieved when the GO content is 0.06%. At this GO content and SF contents of 6%, 8%, and 10%, the compressive strength of the consolidated body increases by 11.13%, 22.40%, and 29.76% respectively, compared with the body without SF. Furthermore, when the GO content is 0.06% and the SF content is 10%, the compressive strength of the consolidated body at 28 days of age reaches its peak, showing an enhancement of 65.06% compared to the C1 group and 21.94% compared to the C2 control group.

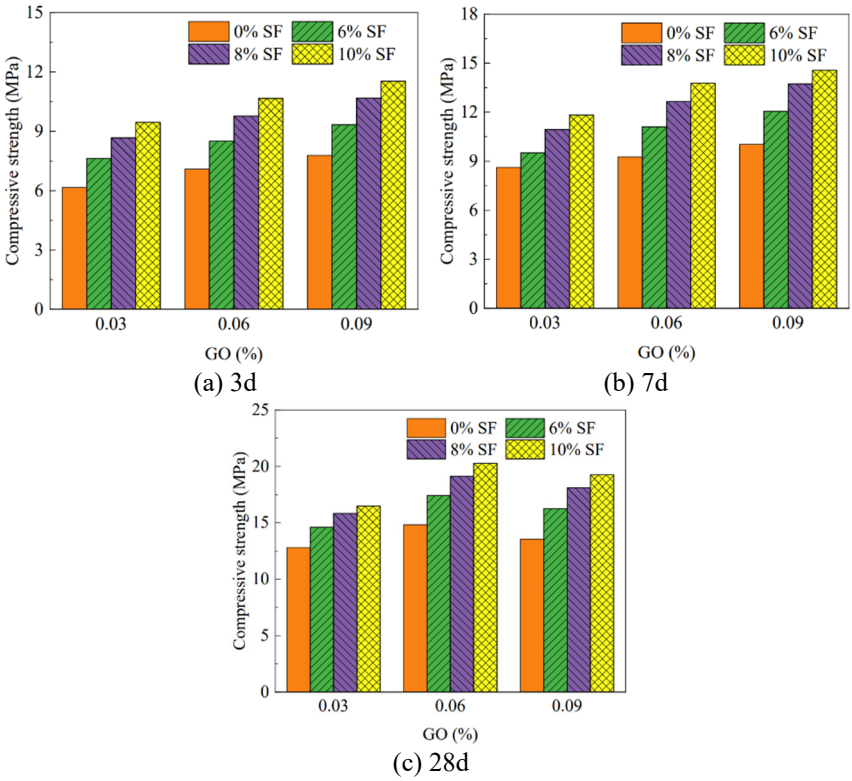

Fig. 6. Variation of compressive strength of solid with GO/SF compounding dosage

(3) Analysis of the Influence of Mechanical Strength of Consolidated Mass by GO/SF Blending.

GO/SF blending significantly improves the flexural and compressive strength of the consolidated body at the early stage. Firstly, because GO and SF have smaller particle size and higher strength and modulus, they can fill micro-pores and micro-cracks between soil particles, hydration products, soil particles and hydration products, and SF can also fill some larger pores and cracks, thus improving the integrity of the structure and improving the early mechanical strength of the consolidated body. In addition, GO can not only promote the hydration reaction of cement and generate a large number of flaky calcium hydroxide crystals, but also adjust the arrangement of hydration products to make the structure more compact. The addition of SF will promote the consumption of calcium hydroxide crystals and generate hydration products such as hydrated calcium silicate gel with higher strength and better crystallinity, which will reduce the porosity of the consolidated body and improve the mechanical strength.

When the content of SF is 0% and 6%, with the increase of GO content, the flexural strength of 7-day-old consolidated body first increases and then decreases, while the compressive strength increases, which indicates that GO may improve the compressive strength better than the flexural strength. When the content of SF is increased to 8%

and 10%, the flexural strength of 7-day-old solidified body increases with the increase of GO content. It is possible that increasing the content of SF can make up for the deficiency of improving the flexural strength of GO. When the content of SF is constant and the content of GO is increased from 0.06% to 0.09%, the flexural strength and compressive strength of the consolidated samples at the age of 28 days decrease. The reason may be that a large amount of SF is consumed by hydration reaction in the early stage, and calcium hydroxide crystals can no longer be consumed in large quantities; The addition of GO easily absorbs a large amount of water, which leads to the increase of pores in the consolidated body, increases the structural defects in the material, and the poor dispersion also reduces the ability of GO to promote hydration reaction.

4 MICROSCOPIC EXPERIMENTAL STUDY

On the basis of the existing research, the changes of impermeability and mechanical strength of the consolidated body before and after adding GO and SF and under different dosage conditions were deeply explored. The pore microstructure of consolidation body with different content of GO and SF was studied by NMR. The porosity and pore distribution of consolidation body with different content of GO and SF were obtained, and the mechanism of impermeability change of consolidation body was understood. Furthermore, X-ray diffraction test was used to quantitatively analyze the chemical composition of the consolidated body under different conditions, revealing the formation of hydration products during the hydration reaction.

4.1 Nuclear Magnetic Resonance

Nuclear magnetic resonance (NMR) is a technology that excites nuclear spins in low energy states by magnetic field and radio frequency field, so as to obtain information about nuclei [29]. In NMR technique, the measurement of relaxation time is usually used to indirectly characterize the change of internal pores of samples. Relaxation time mainly includes longitudinal relaxation time (T_1) and transverse relaxation time (T_2). Because the measurement process of T_2 is short, T_2 spectral curves are usually used to reveal the change process of internal pores in cement-soil samples. T_2 spectral curves can provide a detailed view of pore distribution in samples. By analyzing the data points on these spectral curves, the pore distribution can be accurately depicted, and its conversion relationship is shown in the following equation (4) [30]:

$$\frac{1}{T_2}\rho_2\left(\frac{S}{V}\right) = F_s\frac{\rho_2}{R} \tag{4}$$

Where: R-pore radius;

ρ_2 -T_2 surface relaxation strength is a constant related to soil properties;

F_s -geometric shape factor, for spherical pores, F_s=3, cylindrical pores, F_s=2;

S -pore surface area where water is located;

V -the pore volume in which the water is located.

Therefore, the T_2 spectrum curve of soil sample can reflect the pore size inside the sample, and NMR can be used to test the content and distribution of different pore sizes inside the sample [29]. According to Deng et al. [31] and Horpinbulsu [32], the pore size can be divided into four intervals: micropores ($R \leq 0.01\mu m$), small pores ($0.01\mu m \leq R \leq 0.1\mu m$), mesopores ($0.1\mu m \leq R \leq 1\mu m$) and macropores ($R \geq 1\mu m$).

Fig. 7 shows the T_2 spectrum curves of three groups of consolidated bodies, C1, C2 and G11, at 24h age. According to the basic principle of NMR measurement, the relaxation time T_2 is proportional to the pore size, and the peak area below T_2 spectrum curve represents the pore water content in T_2 range. It can be seen from the figure that there are three peaks in the T_2 curve of all consolidated bodies, which are distributed around 0.01 ~ 8.7 ms, 40 ~ 330ms and 340 ~ 2970ms respectively. The peak of 0.01 ~ 8.7 ms is the most significant, which is listed as the main peak P_1, and the other peaks are classified as secondary peaks P_2 and P_3, and the height change of each peak from left to right in the figure corresponds to the change trend of corresponding pore distribution respectively.

The permeability coefficient is primarily influenced by the presence of large pores, hence the analysis focuses on the distribution of these larger voids. It is observed that at a curing age of 24 h, the solidified body of Group C1 has the highest P_1 peak, corresponding to a larger pore volume and size. In contrast, the solidified body of Group C2 exhibits a lower P_1 peak, indicating smaller pore volume and slightly smaller pore size, with the peak shifted left compared to Group C1. Group G11's solidified body has the lowest P_1 peak, corresponding to the smallest pore volume and size, with the peak also shifted left relative to C1, similar to the optimized group, indicating the smallest pore size. The smaller pore volume and size result in a lower permeability coefficient of the samples, which is consistent with the conclusions drawn from permeability tests.

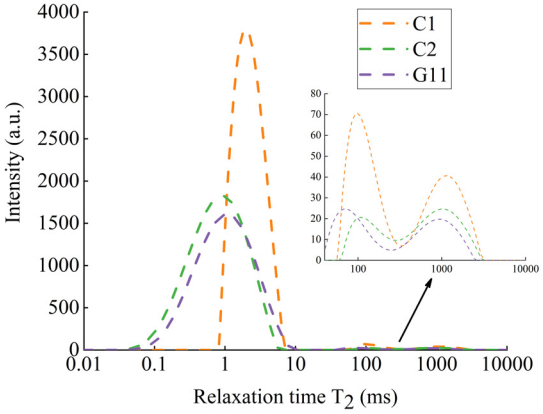

Fig. 7. T_2 curves of different solidified body specimens at 24h age

According to formula (4), the pore size distribution of the samples can be obtained. Fig. 8 shows the distribution schematic of pores of different sizes at a curing age of 24 hours, from left to right, representing micropores, small pores, mesopores, and macropores, respectively. As observed from Fig. 8, the majority of the pore spaces in all samples consist of micropores and small pores, accounting for 97% of the total, with

mesopores and macropores being less prevalent. Compared to Group C1, Group C2 solidified samples show a decreased proportion of small pores and a reduction in mesopores and macropores, but an increased proportion of micropores, indicating that the addition of SF effectively improves the pore distribution, facilitating the transformation of small pores into micropores. In comparison with C2, Group G11 solidified samples exhibit a decrease in small and mesopores, with negligible change in macropores and an increase in micropores, suggesting that GO and SF can synergistically improve the pore structure, thereby reducing the permeability coefficient of the solidified body.

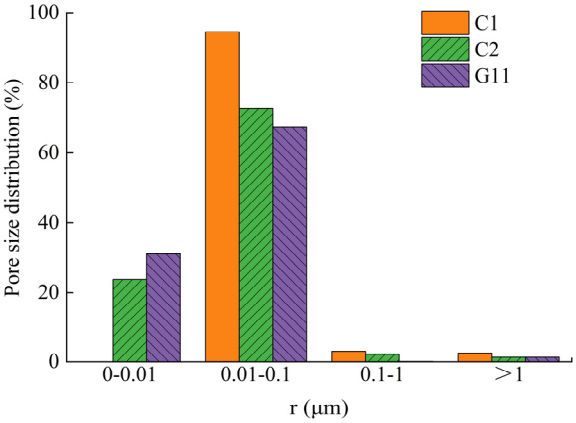

Fig. 8. Pore size distribution of 24h age consolidated specimen

4.2 XRD Analysis

X-ray diffraction test was carried out on the consolidated samples of C1, C2, G2 and G11 after treatment, and the XRD test results of consolidated samples of C1, C2, G2 and G11 at the curing age of 7 days are shown in Fig. 9.

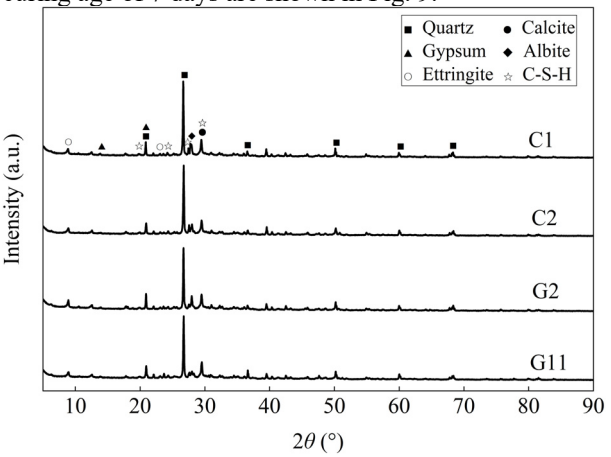

Fig. 9. XRD energy spectrum of solidified body at 7d age

The results in Fig. 9 show that the diffraction patterns of the four groups of consolidated bodies are basically the same, that is, the composition of the phase composition in the solidified soil has not changed, including ettringite, quartz, calcium carbonate, albite and hydrated calcium silicate. This is basically the same as the hydration product of ordinary cement, except that no diffraction peak of calcium hydroxide is found due to pozzolanic reaction between cement and sodium silicate, cement and SF. However, the diffraction peak intensity of the phase corresponding to different batches of consolidated bodies at the same age is different, and it can be clearly seen that the diffraction peak of SiO_2 is the strongest in each consolidated body, which shows that it accounts for the highest proportion in the sample composition. It may be due to the fact that the soil content is the majority in the consolidated body samples of different batches, and the soil samples contain a large number of quartz, so the diffraction peak of SiO_2 is the strongest.

As can be seen from Fig. 9, the addition of SF, GO or the combination of SF and GO will not change the types of hydration products in the consolidated body. From the analysis in the figure, it can be seen that the peak value of the main cement hydration products such as C-S-H which improve the strength of the consolidation body in C2 group of consolidation body samples is higher than that in C1, which shows that the pozzolanic effect of SF promotes the conversion of cement hydration products C-H to C-S-H, and the generated hydration products make the consolidation body closer, thus improving the impermeability and mechanical strength of the consolidation body; Compared with C1, the peak value of C-S-H and other main cement hydration products which improve the strength of cement in G2 consolidated samples is also higher, and the peak value of albite in consolidated samples is obviously higher, which shows that GO can promote the formation of cement hydration products, and at the same time promote the adsorption and exchange reaction between K^+ attached to soil particles and Na^+ in consolidated samples and Ca^+ formed after cement hydration; The peak value of C-S-H in G11 group is the maximum in four groups, and the peak value of ettringite and albite is also significantly higher than that in other three groups, which shows that SF and GO can cooperate to promote the formation of cement hydration products, and the promotion effect is also very obvious. The formation of a large number of cement hydration products can not only better fill the pores between soil particles, but also promote some smaller soil particles to gather closely together and further become larger stone bodies, thus promoting the improvement of impermeability and mechanical strength of stone bodies.

5 CONCLUSION

(1) Incorporating GO into cement-based solidified bodies can significantly reduce their permeability coefficient and enhance early flexural and compressive strengths. The permeability coefficient decreases notably as the GO content increases from 0.03% to 0.09% during the 12 h and 24 h curing periods, with the effect being most pronounced at a 0.06% GO content. In terms of mechanical properties, the addition of GO also increases the flexural and compressive strengths of the solidified body. During the 3 d

curing period, the flexural strength increases with the addition of GO, but during the 7 d and 28 d curing periods, both the flexural and compressive strengths initially increase and then decrease, showing optimal mechanical performance at a 0.06% GO content.

(2) As the addition of GO and SF increases, a decreasing trend in the permeability coefficient of the solidified body is observed. This effect is particularly noticeable when the SF content reaches 10%, indicating its efficacy in reducing the porosity of the solidified body. A significant reduction in the permeability coefficient is also observed even at lower GO content levels. For flexural and compressive strengths, the combined addition of GO and SF positively impacts these mechanical properties. At the 3 d curing period, the solidified body exhibits maximum flexural and compressive strengths with 0.09% GO and 10% SF content. This enhanced effect remains significant up to the 7 d curing period, suggesting that appropriate incorporation of GO and SF can significantly improve the early and mid-term mechanical performance of the solidified body. However, by the 28 d curing period, the growth trend in flexural and compressive strengths begins to slow, indicating a diminished enhancement effect of GO and SF on the mechanical properties of the solidified body over time.

(3) Using NMR technology to analyze the changes in porosity and pore size distribution, it was found that the addition of GO and SF to cement-based materials solidifying silty sand particles effectively reduced the porosity and improved the pore size distribution of the solidified body. More detailed pore size analysis further revealed the optimization of the pore structure under the combined action of GO and SF, providing strong microscopic evidence for its enhanced permeability resistance. XRD analysis confirmed that the addition of GO and SF does not alter the types of hydration products in the solidified body but significantly enhances its performance by optimizing the content and structure of these hydration products.

(4) This study primarily focuses on silty soil, but actual engineering soil layers often consist of more than just silty soil and may include various interlayers. Therefore, it is recommended to further investigate the performance under complex soil conditions. Additionally, while this research is centered on water permeability tests, permeation by alkaline or acidic water is a common phenomenon in real-world engineering environments, necessitating a deeper analysis of the permeability coefficient in alkaline or acidic conditions. Lastly, given that this study is predominantly based on laboratory experiments and real-world engineering conditions are much more complex and uncertain, it is crucial to emphasize the necessity of validating and analyzing the research findings in actual engineering practice.

REFERENCES

1. Zhu Weishen, Zhao Chenglong, Zhou Hao, et al. Thinking and understanding of some key problems in current rock mechanics research [J]. Journal of Rock Mechanics and Engineering, 2015, 34 (4): 649-658.
2. ZHANG Xiao, LI Shu-cai, ZHANG Qing-song et al.Application of key hole grouting method in high pressure fracture water plugging [J]. Journal of Rock Mechanics and Engineering, 2011, 30 (7): 1414-1421.

3. Liu Yuxin, He Junlong, Zheng Liang.Application of pile-buttress combined retaining wall in high fill subgrade [J]. Special Structure, 2020, 37 (06): 30-34.
4. Hamed C A, Seyed L H, Hossein M, et al. The effect of zeolite and cement establishment on the mechanical behavior of expansive soils [J]. Construction and Building Materials, 2020, (prepublish): 121630-.
5. AFRAKOTI P T M, CHOOBBASTI J A, GHADAKPOUR M, et al. Investigation of the effect of the coal wastes on the mechanical properties of the cement-treated sandy soil [J]. Construction and Building Materials, 2020, 239 (C).
6. Wang Zhixin, Mei Junpeng, Li Hainan et al.Strength and impermeability of cement-based materials modified by nano-SiO2 and styrene-butadiene rubber powder [J]. Silicate Bulletin, 2022, 41 (12): 4154-4162.
7. Wang Chaojie, Li Fengyuan, Guo Chengchao et al.Mechanical properties and consolidation mechanism of polymer solidified silt [J]. Journal of Building Materials, 2022, 25 (06): 598-606.
8. Wei Jing. Preparation and properties of cement-based grouting materials modified by carbon nanotubes [J]. Functional Materials, 2022, 53 (08): 8180-8185.
9. Wongkeo W, Thongsanitgarn P, Poon C, et al. Heat of hydraulation of cement pastes containing high-volume fly ash and silica fume [J]. Journal of Thermal Analysis and Calorimetry, 2019, 138 (3): 2065-2075.
10. Juan H, Congmi C, Xiaofen Z, et al. Effect of Silica Fume on the Rheological Properties of Cement Paste with Ultra-Low Water Binder Ratio [J]. Materials, 2022, 15 (2): 554-554.
11. Min W, Hao Y. Effects of polycarboxylate another grafted silica fume on flowability, rheological behavior and mechanical properties of cement-silica fume paste with low water-binder ratio [J]. Construction and Building Materials, 2021, 272.
12. Cai Y, Hou P, Cheng X, et al. The effects of nano-SiO2 on the properties of fresh and hardened cement-based materials through its resolution with silica fume [J]. Construction and Building Materials, 2017, 148770-780.
13. Lun Yunxia, Zheng Fangfang. Effect of steel slag power, fly ash, and silica fume on the mechanical properties and durability of cement mortal [J]. Materials Express, 2019, 9 (9): 1049-1054.
14. Nasr M S, Hussain T H, Kubba H Z, et al. Fluence of using high volume fraction of silica fume on mechanical and durability properties of cement mortal [J]. Journal of Engineering Science and Technology, 2020, 15 (4): 2492-2506.
15. Jiang Yufeng, Chen Yue. Effect of ultrafine wollastonite powder on properties of cement-based materials [J]. Nonmetallic Minerals, 2019, 42 (06): 34-37.
16. He Kui, Deng Ying'er. Experimental study on the impermeability and mechanical properties of silica fume modified cement-based cutoff walls[J]. Yangtze River, 2021, 52(08): 204-207.
17. Yang H, Cui H, Tang W, et al. A critical review on research progress of graph/cement based composites [J]. Composites Part A, 2017, 102273-296.
18. Liu J, Li Q, Xu S. Reinforcing Mechanism of Graphene and Graphene Oxide Sheets on Cement-Based Materials [J]. Journal of Materials in Civil Engineering, 2019, 31 (4): 04019014-04019014.
19. Da C, Hongbin F, Jinghong L. Graphene oxide: preparation, functionalization, and electrochemical applications. [J]. Chemical reviews, 2012, 112 (11): 6027-53.
20. Pan Z, He L, Qiu L, et al. Mechanical properties and microstructure of a graphene oxide-cement composite [J]. Cement and Concrete Composites, 2015, 58140-147.
21. Ren J, Lai Y, Gao J. Exploring the influence of SiO2 and TiO2 nanoparticles on the mechanical properties of concrete [J]. Construction and Building Materials, 2018, 175277-285.

22. Lin C, Wei W, Hu H Y. Catalytic behavior of graphene oxide for cement hydraulation process [J]. Journal of Physics and Chemistry of Solids, 2016, 89128-133.
23. Du H, Pang D S. Enhancement of barrier properties of cement mortar with graphene nanoplatelet [J]. Cement and Concrete Research, 2015, 7610-19.
24. Mokhtar M, Abo-El-Enein S, Hassaan M, et al. Mechanical performance, pore structure and micro-structural characters of graphene oxide nano platelets reinforced cement [J]. Construction and Building Materials, 2017, 138333-339.
25. Mohammed A, Sanjayan J, Duan W, et al. Incorporating graphene oxide in cement composites: A study of transport properties[J]. Construction and Building Materials,2015,84341-347.
26. KULANTHAIVEL P, SOUNDARA B, VELMURUGAN S, et al. Experiential investigation on establishment of clay oil using nano-materials and white cement [J]. Materials Today: Proceedings, 2021, 45: 507-511.
27. AVCI E, DEVECI E, GOKCE A. Effect of Sodium Silicate on the Strength and Permeability Properties of Ultimate Cement Grouted Sands [J]. Journal of Materials in Civil Engineering, 2021, 33 (8): 4021203.
28. Do H, Pham V, Nguyen H, et al. Prediction of Unconfined Compressed Strength and Flexural Strength of Cement-Stabilized Sandy Soils: A Case Study in Vietnam [J]. Geotechnical and Geological Engineering, 2021, 39 (7): 1-16.
29. Cheng Fuzhou, Lei Xuewen, Meng Qingshan et al. Study on pore water content and distribution of dredged silt solidified soil based on nuclear magnetic resonance technology [J]. Proceedings of Yangtze River Academy of Sciences, 2016, 33 (10): 116-120.
30. Ma Denghui. Study on the deterioration mechanism of physical and mechanical properties of rocks by water-rock interaction [D]. Hefei University of Technology, 2020.
31. Deng Y, Yue X, Liu S, et al. Hydraulic conductivity of cement-stabilized marine clay with metakaolin and its correlation with pore size distribution [J]. Engineering Geology, 2015, 193146-152.
32. Horpibulsuk S, Rachan R, Raksachon Y. Role of Fly Ash on Strength and Microstructure Development in Blended Cement Stabilized Silty Clay [J]. Soils and Foundations, 2009, 49 (1): 85-98.